J. Phys. B: At. Mol. Opt. Phys. **31** (1998) 4205–4224. Printed in the UK PII: S0953-4075(98)93286-2

Electron-impact excitation of the $3\,^2$D state of sodium from the optically prepared $3\,^2$P state

M Shurgalin, A J Murray, W R MacGillivray† and M C Standage

Laser Atomic Physics Laboratory, School of Science, Griffith University, Nathan, Qld, 4111, Australia

Received 15 April 1998, in final form 29 June 1998

Abstract. An experimental investigation of electron-impact excitation of the $3\,^2$D-state from the laser-excited $3\,^2$P state of atomic sodium is reported for 30 eV incident electron energy. A detailed consideration of the measurement technique is presented, based on the density matrix description of electron-impact-induced atomic transitions for target atoms in which the spin of the target electron is unchanged. It is shown that some inference about excitation probabilities between individual magnetic substates of the P- to D-state transition can be made from measurements of the four pseudo-Stokes parameters. A description of the inelastic scattering experiment and an analysis of the experimental measurements in terms of both the standard atomic collision parameters and magnetic substate excitation probabilities are presented. Convergent close-coupling theoretical calculations are compared with the experimental results and show good agreement.

1. Introduction

Over the last two decades considerable progress has been made in the fundamental understanding of electron-impact excitation of atoms. Both the development of better theoretical treatments of the scattering problem and new experimental methods have contributed to this progress (Andersen *et al* 1997a, b, 1988, Andersen and Bartschat 1996). However, most of these investigations have been concerned with electron-impact excitation of atoms from the ground state. The studied transitions have, in most cases, been between states with $L = 0$ and 1 angular momenta (S- and P-states). There has been less work, either experimental or theoretical, performed on the electron-impact excitation of D-states (e.g. Andersen and Bartschat 1997 and references therein, Verma and Srivastava 1996 and references therein) and on inelastic electron scattering from excited atoms (Trajmar and Nickel 1993, Lin and Anderson 1992). Meanwhile, the availability of experimental data has played a major role in the development of the theoretical models. The relatively small amount of experimental data available for electron-impact-induced transitions between excited atomic states has recently stimulated considerable interest in experimental studies in this area (e.g. Zetner *et al* 1997).

Experimental techniques developed for the investigation of electron-impact excitation of an atomic P-state from a ground S-state enable different sets of experimental observables to be obtained with which to test theories. Apart from measuring differential cross

† E-mail address: W.MacGillivray@sct.gu.edu.au

0953-4075/98/184205+20$19.50

sections (DCSs), atomic-collision parameters (ACPs) can be measured (Andersen *et al* 1988, Andersen and Bartschat 1997) which are related to individual scattering amplitudes and thus provide finer details about the scattering process. The combination of both DCS and ACP measurements provides for more comprehensive tests of different theoretical models. However, characterization of ACPs for transitions between excited atomic states with higher angular momenta has not been developed to the same extent as for S- to P-state transitions. This can be explained by the fact that increasing the angular momentum of the states involved in electron-impact-induced transitions leads to a substantial increase in the number of individual scattering amplitudes required to fully characterize the scattering process. Accordingly, defining the experimentally measurable quantities and the techniques for measuring these quantities becomes more complex and difficult. As an example, for electron-impact-induced transitions between P- and D-states of sodium where the total spin is conserved, the number of scattering amplitudes in each total spin channel increases to eight, in comparison with only two scattering amplitudes for an S- to P-state transition (Andersen and Bartschat 1996).

One of the first experiments to measure ACPs for electron-impact-induced transitions between excited P- and D-states was performed by Hermann (1979) for sodium atoms at 5 eV incident electron energy. These data were not published until the review of Andersen *et al* (1988) made the results available. The experiment involved the preparation of the 3P excited state of sodium with polarized laser radiation and the measurement of pseudo-Stokes parameters, which are the relative differences in differential cross sections for different laser polarizations, for the 3P- to 3D-state transition. No analysis was made of the electron-impact-excited 3D-state. Such an experiment is equivalent to one in which the 'isotropic' D-state is de-excited to the P-state following superelastic electron scattering. The isotropic D-state has all magnetic substates equally populated with no coherences between them. 'Standard' ACPs for the electron-impact-excited P-state were obtained and a discussion in the framework of these ACPs was presented (Andersen *et al* 1988). A theoretical calculation, using the convergent close-coupling method (CCC) was presented by Bray *et al* (1994). The CCC calculations proved to be in good agreement with the experimental data.

Recently, similar work has been performed for barium atoms at 20 eV incident electron energy (Li and Zetner 1995, 1996). A number of ACPs were measured and a comparison was made with theoretical calculations utilizing the unitarized distorted-wave approximation. Also the relationship between ACPs and the partial differential cross sections (PDCS) (Hummer and Burns 1986, Csanak *et al* 1992, Li *et al* 1994) and the practical significance of the latter quantities were discussed.

In the work presented in this paper, a general description of electron-impact-induced transitions between states of different angular momenta is developed, based on the density matrix formalism. Atomic species are considered where the total spin is conserved during the collision. The incident electrons are spin-unpolarized and no spin analysis is carried out for the final states. Measurement techniques are considered for studying electron-impact excitation of a D-state from a P-state together with a discussion of the information that can be obtained. An experiment is described in which inelastic scattering from the laser-excited $3\,^2P_{3/2}$ state of a sodium atom occurs. The experimental data are presented and analysed for excitation to the $3\,^2D$-state using 30 eV incident electron energy. Certain sums of magnetic substate excitation probabilities are obtained and discussed. Standard ACPs are also deduced from the measurements for the corresponding 'time-inverse' de-excitation process from the 3D isotropic state for the corresponding 28.4 eV incident electron energy.

2. Theory

For electron collisions with light atoms such as sodium, a well justified and in some cases experimentally verified assumption that significantly simplifies the description of the scattering process is that the spin of the projectile electron is unchanged during the collision. This assumption follows from the neglect of explicit spin–orbit interaction forces involving the projectile and target atom electrons and spin–orbit coupling inside the target atom. The explicit spin–orbit interaction, as can be seen from Dirac's equation (Kessler 1985), is proportional to the charge of the nucleus and hence becomes significant only for heavier atoms, such as mercury. Spin–orbit coupling inside the atom, resulting in fine and hyperfine structure, is also a weak interaction for light atoms in comparison with the collisional interaction and thus can be neglected during the collision (Andersen *et al* 1988). Therefore, the description of collisionally induced transitions in $|L\, m_L\, S\, m_S\rangle$ representation is appropriate and the transformation of the density matrices of the initial and final states from and to hyperfine structure representation can be made through the application of standard quantum angular momentum coupling algebra. With the total electron spin conserved, two separate total spin channels arise in the scattering process for atoms with a single valence electron. Furthermore, if projectile electrons are not spin-unpolarized and no spin analysis is performed on final states, averaging over spins can be performed. The following general formula, the derivation of which is outlined in the appendix, describes the relationship between the initial and final density matrix elements:

$$\rho^{A(2)}_{MN} = \sum_{mn} \rho^{A(1)}_{mn} \sum_{S} W_S T_{S,Mm} T^*_{S,Nn} \tag{1}$$

where $\rho^{A(2)}_{MN}$ and $\rho^{A(1)}_{mn}$ are the density matrices of the final and initial states, S is the total electron spin, $W_S = (2S + 1)/2(2S_0 + 1)$ is the probability of scattering through each total spin channel, S_0 is the atomic electron spin and $T_{S,ij}$ are the spin-averaged scattering amplitudes (or transition operator matrix elements) for each total spin channel S. In this formula, the spin-averaged scattering amplitudes have no dependence on spin variables. The formula is valid in general for states with arbitrary atomic orbital angular momentum. For example, if the initial state is an S-state described by a density matrix normalized to unity, $\rho^{A(1)}_{00} = 1$, and expression (1) simplifies to

$$\rho^{A(2)}_{MN} = \sum_{S} W_S T_{S,M0} T^*_{S,N0}. \tag{2}$$

Powerful symmetry considerations can be used to determine the non-zero matrix elements $T_{S,Mm}$. Since the scattering plane has reflection symmetry for the scattering process, certain invariance principles must be obeyed (Andersen *et al* 1988, Blum and Kleinpoppen 1979). The most general argument to consider is the reflection invariance of the total wavefunction of the two colliding particles (Hermann and Hertel 1982b). The total wavefunction consists of both orbital and spin components. If one component changes its reflection symmetry in the collision then the other one must also change. Since the total spin is conserved, the spin component of the total wavefunction retains its initial reflection symmetry. Therefore, only those orbital states that have the same reflection symmetry as the initial orbital states will be excited and contribute to the density matrix of the excited atoms. Accordingly, the only non-zero transition matrix elements in equation (1) are between orbital states of the same reflection symmetry. Figure 1 provides an illustration of this argument for P- to D-state transitions, where P- and D-orbitals are shown in the natural frame of reference (Hermann and Hertel 1982a) and the possible collision-induced transitions are indicated by arrows.

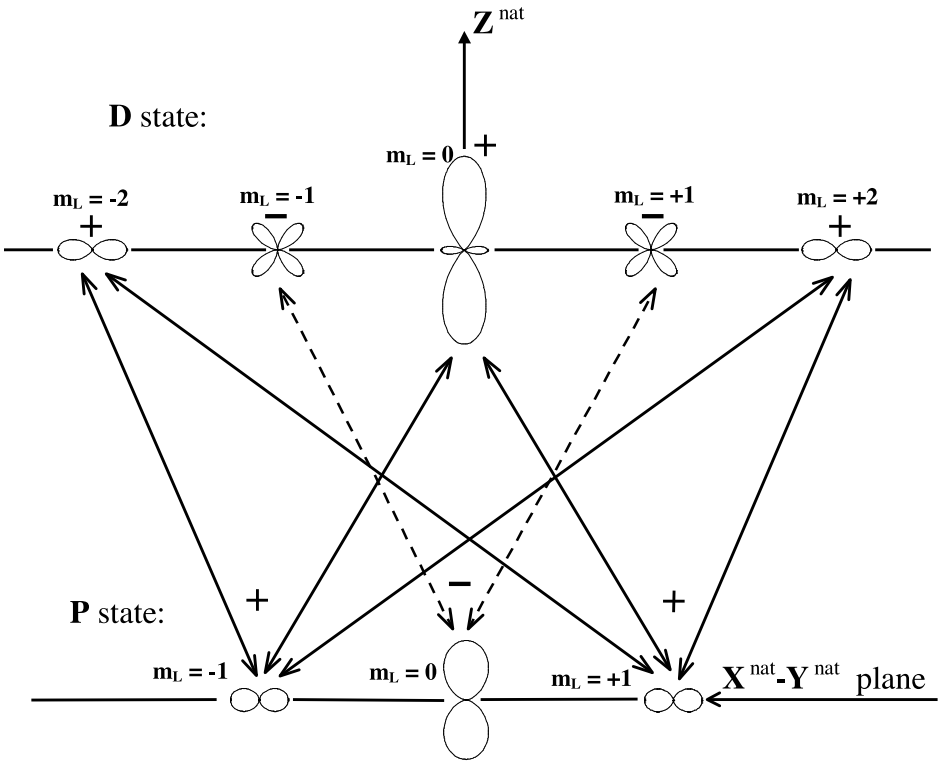

Figure 1. Illustration of the symmetry properties of the transition operator. Atomic orbitals are shown in the natural frame of reference. + and − indicate the positive and negative reflection symmetry of atomic orbitals and arrows indicate the allowed transitions.

Another powerful symmetry for the transition operator is the time-reversal symmetry. Figure 2 depicts a scattering process resulting in the transition of the system of target atoms and projectile electrons from an initial state ρ^i to a final state ρ^f and the scattering process which is obtained by the reversal of time. In the time-inverse scattering process the system is returned from the ρ^f state exactly into the ρ^i state according to the principle of micro-reversibility. Both time-direct and time-inverse processes can be represented by the $\boldsymbol{S}$-matrix equations as follows:

$$\begin{aligned} &\text{time-direct:} \quad \rho^f = \boldsymbol{S}\,\rho^i\,\boldsymbol{S}^+ \\ &\text{time-inverse:} \quad \rho^i = \boldsymbol{S}^D\,\rho^f\,\boldsymbol{S}^{D+} \end{aligned} \tag{3}$$

where $\boldsymbol{S}$ and $\boldsymbol{S}^D$ are the scattering matrices for the time-direct excitation process and time-inverse de-excitation process, respectively. From these equations it follows that $\boldsymbol{S}\boldsymbol{S}^D = \boldsymbol{1}$ and $\boldsymbol{S}^+\boldsymbol{S}^{D+} = \boldsymbol{1}$. Using the unitary property of the scattering matrix $\boldsymbol{S}^{-1} = \boldsymbol{S}^+$ (Messiah 1962) the relationship between the two scattering matrices is obtained: $\boldsymbol{S}^D = \boldsymbol{S}^{-1} = \boldsymbol{S}^+$ and $\boldsymbol{S}^{D+} = (\boldsymbol{S}^+)^{-1} = \boldsymbol{S}$. From these equations the relationship between the transition operators can be established. Since the transition operator is related to the scattering operator by $\boldsymbol{T} = \boldsymbol{S} - \boldsymbol{1}$ and both operators satisfy the distribution law $(\boldsymbol{A}+\boldsymbol{B})^+ = \boldsymbol{A}^+ + \boldsymbol{B}^+$ (Blum 1981, Messiah 1962), the following holds for the transition matrices $\boldsymbol{T}$ and $\boldsymbol{T}^{\text{deex}}$ of the

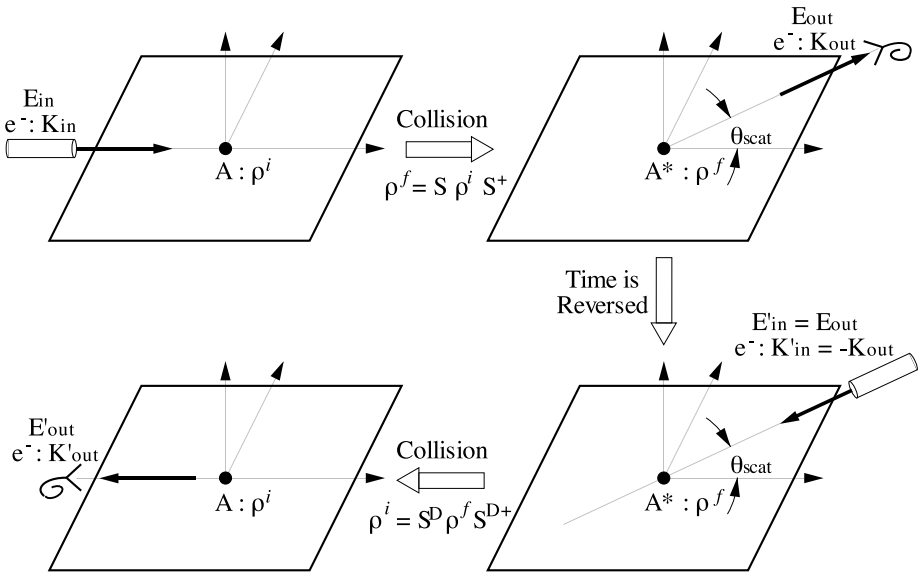

Figure 2. Illustration of the time-reversal symmetry of the transition operator.

time-direct (excitation) and time-inverse (de-excitation) processes, respectively:

$$\boldsymbol{T}^{\text{deex}}(E_0-\Delta,\theta_{\text{scat}})=\boldsymbol{T}^{+}(E_0,\theta_{\text{scat}}) \qquad \boldsymbol{T}^{\text{deex}+}(E_0-\Delta,\theta_{\text{scat}})=\boldsymbol{T}(E_0,\theta_{\text{scat}}) \tag{4}$$

where E_0 denotes the incident energy, Δ is the energy loss and θ is the scattering angle. This relationship expresses the principle of micro-reversibility that is exploited in the superelastic technique. It is apparent that the incident electron energy in the time-inverse process is less by the energy loss of the transition involved than the incident energy in the time-direct process.

The time-inverse de-excitation process can be described by the following formula, similar to equation (A5):

$$\rho^{(1)}=\boldsymbol{T}^{\text{deex}}\rho^{(2)}\,\boldsymbol{T}^{\text{deex}+}. \tag{5}$$

Then, in the same way that the matrix equation (1) is obtained (see the appendix, equation (A5)), the following equation, describing the time-inverse transition, is derived from (5):

$$\rho^{(1)}_{mn}=\sum_{MN}\rho^{(2)}_{MN}\sum_{S}W_S\;T^{\text{deex}}_{S,mM}\;T^{\text{deex}^*}_{S,nN}=\sum_{MN}\rho^{(2)}_{MN}\sum_{S}W_S\;T^{*}_{S,Mm}\;T_{S,Nn} \tag{6}$$

where

$$T^{\text{deex}}_{S,mM}(E_0-\Delta,\theta)=T^{+}_{S,mM}(E_0,\theta)=T^{*}_{S,Mm}(E_0,\theta)$$

and

$$T^{\text{deex}^*}_{S,nN}(E_0-\Delta,\theta)=T^{\text{deex}+}_{S,Nn}(E_0-\Delta,\theta)=T_{S,Nn}(E_0,\theta)$$

follow from expression (4). The probabilities W_S for each total spin channel remain the same for the time-inverse case. The symmetry of the transition operator with respect to time reversal allows ACPs to be obtained through the electron-impact de-excitation of atoms initially prepared in some known excited state. This method has been used in the superelastic method for studies of S- to P-state transitions (Andersen *et al* 1988). Now we shall examine

how this symmetry can be exploited for studies of electron-impact transitions between P- and D-states.

Consider the excitation of the D-state from the optically prepared P-state:

$$\rho_{MN}^{D(e)} = \sum_{mn} \rho_{mn}^{P(o)} \sum_{S} W_S \overset{\mathrm{P}\to\mathrm{D}}{T}_{S,Mm} \overset{\mathrm{P}\to\mathrm{D}}{T}{}^{*}_{S,Nn}(E_0) \tag{7}$$

where E_0 denotes the incident electron energy and the superscripts denote the atomic states and excitation process, (e) for electron-impact excitation and (o) for the optical excitation with laser light. The differential cross section for the D-state excitation from the P-state is given by the trace of $\rho^{D(e)}$:

$$S = \mathrm{tr}\left(\rho_{MN}^{D(e)}\right) = \sum_{mn} \rho_{mn}^{P(o)} \sum_{M} \sum_{S} W_S \overset{\mathrm{P}\to\mathrm{D}}{T}_{S,Mm} \overset{\mathrm{P}\to\mathrm{D}}{T}{}^{*}_{S,Mn}(E_0). \tag{8}$$

Consider now the excitation of the P-state from an isotropic D-state, i.e. a D-state with equally populated magnetic substates and no coherences, in the time-inverse geometry, performed at the incident energy $E_0 - \Delta$, which is described by the following equation:

$$\rho_{mn}^{P(e)} = \sum_{M} \sum_{S} W_S \overset{\mathrm{D}\to\mathrm{P}}{T}_{S,mM} \overset{\mathrm{D}\to\mathrm{P}}{T}{}^{*}_{S,nM}(E_0 - \Delta) \tag{9}$$

where Δ denotes the energy separation between the P- and D-states and the density matrix of the initial D-state is normalized to unity. From the time-inverse symmetry discussed above it follows that

$$\rho_{mn}^{P(e)} = \sum_{M} \sum_{S} W_S \overset{\mathrm{P}\to\mathrm{D}}{T}{}^{*}_{S,Mm} \overset{\mathrm{P}\to\mathrm{D}}{T}_{S,Mn}(E_0) \tag{10}$$

and consequently equation (8) becomes ($\rho_{mn}^{P(e)^*} = \rho_{nm}^{P(e)}$):

$$S = \sigma_{\mathrm{tot}} \sum_{mn} \rho_{nm}^{P(e)} \rho_{mn}^{P(o)} \tag{11}$$

where, instead of the normalization of the density matrix of the isotropic D-state, the normalization of $\rho^{P(e)}$ is used instead $\left(\rho_{11}^{P(e)} + \rho_{00}^{P(e)} + \rho_{-1-1}^{P(e)} = 1\right)$, and the DCS σ_{tot} is introduced to account for the density matrix normalizations. For a P-state there are four independent density matrix elements of $\rho^{P(e)}$: $\rho_{11}^{P(e)}$, $\rho_{00}^{P(e)}$, $\rho_{-1-1}^{P(e)}$ and $\rho_{1-1}^{P(e)}$ (note that $\rho_{1-1}^{P(e)} = \rho_{-11}^{*P(e)}$).

Diagonal elements of $\rho^{P(e)}$ give the probabilities of excitation of a D-state magnetic substate from a certain magnetic substate of the P-state (magnetic substate excitation probabilities are written here as MSEPs) at the incident electron energy E_0:

$$\begin{aligned}
\rho_{11}^{P(e)} &= \sum_{M} \sigma_{M1} = \sigma_{-21} + \sigma_{01} + \sigma_{21} \\
\rho_{00}^{P(e)} &= \sum_{M} \sigma_{M0} = \sigma_{-10} + \sigma_{10} \\
\rho_{-1-1}^{P(e)} &= \sum_{M} \sigma_{M-1} = \sigma_{-2-1} + \sigma_{0-1} + \sigma_{2-1}
\end{aligned} \tag{12}$$

where the probabilities σ_{Mm} are defined as

$$\sigma_{Mm} = \frac{1}{\sigma_{\mathrm{tot}}} \sum_{S} W_S \left| \overset{\mathrm{P}\to\mathrm{D}}{T}_{S,Mm} \right|^2. \tag{13}$$

σ_{Mm} are related to partial differential cross sections (PDCS) for each pair of magnetic substates m and M of the initial and final states, respectively, in the natural frame of reference as

$$\mathrm{PDCS}_{Mm} = \sigma_{\mathrm{tot}}\, \sigma_{Mm} \tag{14}$$

where σ_{tot} is the differential cross section of the D-state excitation from the P-state.

Scattering from an optically prepared P-state allows the determination of a number of the summation terms σ_{Mm} as given in equation (12). These sums do not provide detailed information on individual spin-averaged scattering amplitudes, however, they allow for a more comprehensive comparison with theory than DCS measurements and in this sense can be termed ACPs.

Standard techniques for the optical preparation of the P-state and measurements of the pseudo-Stokes parameters (Farrell *et al* 1991, Sang *et al* 1994) are used to determine the density matrix elements $\rho^{P(e)}$ in equation (11) and thus the sums σ_{Mm}. Perpendicular and co-planar laser excitation geometries are required for measuring four pseudo-Stokes parameters. In the perpendicular geometry the laser beam is propagated perpendicular to the scattering plane and three pseudo-Stokes parameters are defined in the following way:

$$P_1^S = \frac{S(0) - S(90)}{S(0) + S(90)} \qquad P_2^S = \frac{S(45) - S(135)}{S(45) + S(135)} \qquad P_3^S = \frac{S(\mathrm{RHC}) - S(\mathrm{LHC})}{S(\mathrm{RHC}) + S(\mathrm{LHC})}. \tag{15}$$

$S(\varphi)$ is the count rate of the electrons scattered from the target atoms excited with linearly polarized laser light with the polarization vector at angle φ to the direction of the incident electron beam. S(RHC) and S(LHC) are the count rates of the electrons scattered from the target atoms excited with right- and left-hand circularly polarized laser light, respectively. In co-planar geometry the laser beam is propagated in the scattering plane and the fourth pseudo-Stokes parameter is defined in the following way:

$$P_4^S = \frac{S(\parallel) - S(\perp)}{S(\parallel) + S(\perp)} \tag{16}$$

where $S(\parallel)$ and $S(\perp)$ are the count rates of the electrons scattered from the target atoms excited with linearly polarized laser light with the polarization vector in the scattering plane and perpendicular to the scattering plane, respectively. Figure 3 provides an illustration of the scattering and laser excitation geometries used for pseudo-Stokes parameter measurements.

To relate the pseudo-Stokes parameters (15) and (16) to matrix elements $\rho^{P(e)}$, a laser frame of reference is used (Farrell *et al* 1991), which has a quantization axis along the polarization vector for linearly polarized light and along the direction of propagation of the laser beam for circularly polarized light. In the laser frame of reference, the density matrix of the ensemble of optically excited atoms is diagonal due to selection rules, thus providing a simpler form of equation (11). In the laser frame of reference equation (11) becomes

$$S = \sum_m \rho_{mm}^{P(e)\,\mathrm{LF}} \rho_{mm}^{P(o)\,\mathrm{LF}} \tag{17}$$

where additional superscripts LF denote the density matrix elements in the laser frame of reference.

Excitation with linearly polarized light is considered first. Since all atoms are initially in thermal equilibrium and all magnetic substates of the ground state are equally populated, $\rho_{11}^{3P(o)\,\mathrm{LF}} = \rho_{-1-1}^{3P(o)\,\mathrm{LF}}$ due to the symmetry of the excitation process with respect to the $m = 0$ magnetic substate. Let $\rho_{11}^{3P(o)\,\mathrm{LF}}$ and $\rho_{-1-1}^{3P(o)\,\mathrm{LF}}$ be denoted by a and $\rho_{00}^{3P(o)\,\mathrm{LF}}$ by b, where in the $|L\, m_L\rangle$ representation $a \neq 0$ due to the influence of the hyperfine structure. Then

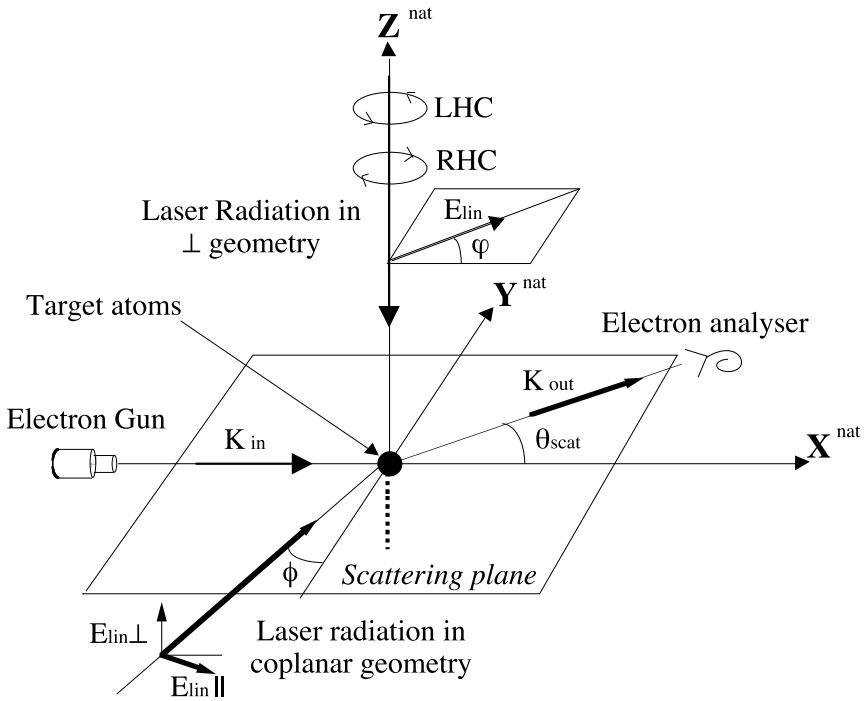

Figure 3. Illustration of the scattering geometry, and perpendicular and co-planar laser excitation geometries used for pseudo-Stokes parameter measurements. The natural frame of reference $X^{\rm nat}$, $Y^{\rm nat}$, $Z^{\rm nat}$ is shown. $\boldsymbol{E}_{\rm lin}$ denotes the directions of linear polarization used for measuring P_1^S, P_2^S and P_4^S parameters.

equation (17) for the differential cross section of scattering from the 3P laser-excited state in the laser frame of reference is

$$S = a\rho_{-1-1}^{3P(e)\,\mathrm{LF}} + b\rho_{00}^{3P(e)\,\mathrm{LF}} + a\rho_{11}^{3P(e)\,\mathrm{LF}} \tag{18}$$

and in the natural frame of reference:

$$S(\varphi) = \tfrac{1}{2}(a+b)\left(\rho_{11}^{3P(e)} + \rho_{-1-1}^{3P(e)}\right) + a\rho_{00}^{3P(e)} + (a-b)\,\mathrm{Re}\left(\rho_{1-1}^{3P(e)}\right)\cos(2\varphi) + (a-b)\,\mathrm{Im}\left(\rho_{1-1}^{3P(e)}\right)\sin(2\varphi) \tag{19}$$

where φ is the angle between the direction of the laser polarization and the $X^{\rm nat}$ axis of the natural frame of reference, which is along the direction of the incident electron beam (figure 3). The density matrix elements $\rho^{P(e)}$ in the natural frame are obtained by application of the matrix transformation rules under reference frame rotations (Farrell *et al* 1991).

The pseudo-Stokes parameters P_1^S and P_2^S are then related to the density matrix elements $\rho_{mn}^{3P(e)}$ as follows:

$$P_1^S = \frac{-2\,\mathrm{Re}\left(\rho_{1-1}^{3P(e)}\right)(b-a)}{(a+b)+(a-b)\rho_{00}^{3P(e)}} \tag{20a}$$

$$P_2^S = \frac{2\,\mathrm{Im}\left(\rho_{1-1}^{3P(e)}\right)(b-a)}{(a+b)+(a-b)\rho_{00}^{3P(e)}} \tag{20b}$$

and the pseudo-Stokes parameter P_4^S is

$$\begin{aligned} P_4^S = \big[&(b-a)+(a+b)\big(P_1^S\cos(2\phi)+P_2^S\sin(2\phi)\big)\\ &+(a-b)\big(P_1^S\cos(2\phi)+P_2^S\sin(2\phi)+3\big)\rho_{00}^{3P(e)}\big]\\ &\times\big[(3a+b)+(a+b)\big(P_1^S\cos(2\phi)+P_2^S\sin(2\phi)\big)\\ &+(b-a)\big(1-P_1^S\cos(2\phi)-P_2^S\sin(2\phi)\big)\rho_{00}^{3P(e)}\big]^{-1} \end{aligned} \tag{20c}$$

where ϕ is the angle between the laser polarization vector and the X^{nat} axis of the natural frame of reference in the co-planar laser geometry when the laser polarization vector is in the scattering plane.

The optical pumping parameter for the linear polarization is given by

$$K_L = \frac{b-a}{b+a} \tag{21}$$

and after some algebraic manipulations it follows from (20) that

$$\begin{aligned} -2\,\mathrm{Re}\big(\rho_{1-1}^{3P(e)}\big) &= \frac{P_1^S}{K_L} - P_1^S\rho_{00}^{3P(e)}\\ 2\,\mathrm{Im}\big(\rho_{1-1}^{3P(e)}\big) &= \frac{P_2^S}{K_L} - P_2^S\rho_{00}^{3P(e)}\\ \rho_{00}^{3P(e)} &= \frac{\big(P_1^S\cos(2\phi)+P_2^S\sin(2\phi)\big)\big(1-P_4^S\big)+K_L-P_4^S(2-K_L)}{K_L\big(4-\big(1-P_4^S\big)\big(1-P_1^S\cos(2\phi)-P_2^S\sin(2\phi)\big)\big)}. \end{aligned} \tag{22}$$

Excitation with circularly polarized laser light can be analysed in a similar manner. Let the density matrix elements $\rho_{11}^{3P(o)\,\mathrm{LF}}$, $\rho_{-1-1}^{3P(o)\,\mathrm{LF}}$ and $\rho_{00}^{3P(o)\,\mathrm{LF}}$ of the ensemble of optically excited atoms in $|L\,m_L\rangle$ representation be denoted by α^+, β^+ and γ^+, respectively, in the case of left-hand circular polarization and α^-, β^- and γ^- in the case of right-hand circular polarization, where all terms are not zero due to the influence of the hyperfine structure. The differential cross section for scattering from the laser-excited atoms, given by the expression (17), is written in the laser frame of reference in the following way:

$$S^{\pm} = \alpha^{\pm}\rho_{11}^{3P(e)\,\mathrm{LF}} + \beta^{\pm}\rho_{-1-1}^{3P(e)\,\mathrm{LF}} + \gamma^{\pm}\rho_{00}^{3P(e)\,\mathrm{LF}} \tag{23}$$

and in the natural frame of reference:

$$S^{\pm} = \alpha^{\pm}\rho_{-1-1}^{3P(e)} + \beta^{\pm}\rho_{11}^{3P(e)} + \gamma^{\pm}\rho_{00}^{3P(e)}. \tag{24}$$

Due to the symmetry of the excitation process with respect to magnetic substates with negative m and positive m, and since all hyperfine substates of the ground state are populated equally (atoms are initially in thermal equilibrium), it follows that $\alpha^+ = \beta^-$, $\gamma^+ = \gamma^-$ and $\beta^+ = \alpha^-$ (a rigorous model of the excitation process shows this explicitly, Farrell *et al* 1988). The P_3^S pseudo-Stokes parameter is then related to the density matrix elements $\rho_{mn}^{3P(e)}$ as follows:

$$P_3^S = \frac{S^- - S^+}{S^- + S^+} = \frac{\big(\alpha^+ - \beta^+\big)\big(\rho_{11}^{3P(e)} - \rho_{-1-1}^{3P(e)}\big)}{\big(\alpha^+ + \beta^+\big)\big(1-\rho_{00}^{3P(e)}\big) + 2\gamma^+\rho_{00}^{3P(e)}}. \tag{25}$$

The optical pumping parameters for excitation with circularly polarized laser light are given by

$$K_c = \frac{\big(\alpha^+ - \beta^+\big)}{\alpha^+ + \beta^+} \qquad \text{and} \qquad K_c'' = \frac{1-3\gamma^+}{1-\gamma^+}. \tag{26}$$

Equation (25) becomes

$$P_3^S = \frac{K_c\left(\rho_{11}^{3P(e)} - \rho_{-1-1}^{3P(e)}\right)}{\left(1 - K_c''\rho_{00}^{3P(e)}\right)} \tag{27}$$

The density matrix elements $\rho_{11}^{3P(e)}$ and $\rho_{-1-1}^{3P(e)}$ are then derived,

$$\begin{aligned}\rho_{11}^{3P(e)} &= \frac{1}{2} + \frac{P_3^S}{2K_c} - \left(\frac{1}{2} + \frac{K_c'' P_3^S}{2K_c}\right)\rho_{00}^{3P(e)} \\ \rho_{-1-1}^{3P(e)} &= \frac{1}{2} - \frac{P_3^S}{2K_c} - \left(\frac{1}{2} - \frac{K_c'' P_3^S}{2K_c}\right)\rho_{00}^{3P(e)}.\end{aligned} \tag{28}$$

Clearly, an accurate knowledge of the optical pumping parameters is very important for the correct determination of the ACPs or MSEPs from the measured pseudo-Stokes parameters. The K_L, K_c and K_c'' parameters are determined from the quantities $\alpha^+, \beta^+, \gamma^+, a$ and b, which in turn depend on the populations of the hyperfine structure substates and their coherences. Theoretical modelling of the laser excitation process using a full quantum electrodynamic treatment that enables the optical pumping parameters to be obtained for different pumping conditions and techniques for their experimental verification have been considered in Farrell *et al* (1988, 1991), Meng *et al* (1992) and Shurgalin *et al* (1998).

3. Experiment

Figure 4 shows a schematic of the experimental apparatus. An electron spectrometer and an atomic beam oven with cold trap are located in a vacuum chamber, pumped by a 500 l s^{-1} turbo-molecular pump. The base pressure in the chamber was less than 10^{-7} mbar. Three orthogonal Helmholtz coils together with mu-metal shielding inside the chamber reduce magnetic fields in the centre of the chamber to less than 0.8 μT in any direction.

The electron spectrometer consists of an electron gun equipped with a hemispherical electron energy selector and a hemispherical scattered electron energy analyser. The overall system resolution achieved was approximately 140 meV FWHM and the incident electron beam current obtained was about 150 nA at an energy of 30 eV. The angular resolution of the spectrometer was estimated to be less than 5°.

Figure 5 shows a typical energy loss spectrum obtained with this spectrometer. A multiple Gaussian curve is fitted to the data. Gaussian curve fitting for the energy loss spectra was used to distinguish the peak corresponding to the 3P–3D transition and the adjacent small peak corresponding to the 3P–4P transition (Stumpf and Gallagher 1985). Curve fitting also allowed the automatic subtraction of any background counts.

The sodium atomic beam oven is of a standard heated crucible type. The oven is equipped with a collimator. A cold trap inside the collimator is used to condense the uncollimated sodium atoms. The collimated sodium atomic beam is dumped onto the main cold trap which is separated from the oven collimator by about 50 mm. By using the collimator an atomic beam of good quality is created, which is well defined in space, with a Doppler width of approximately 100 MHz. Furthermore, the collimation resulted in a low level of background sodium vapour in the chamber. The pressure in the vacuum chamber with the atomic beam oven running was less than 3×10^{-7} mbar. The collimated atomic beam is located in the scattering plane, defined by the incident and the scattered electron directions (see also figure 3), at 90° to the incident electron beam and is therefore

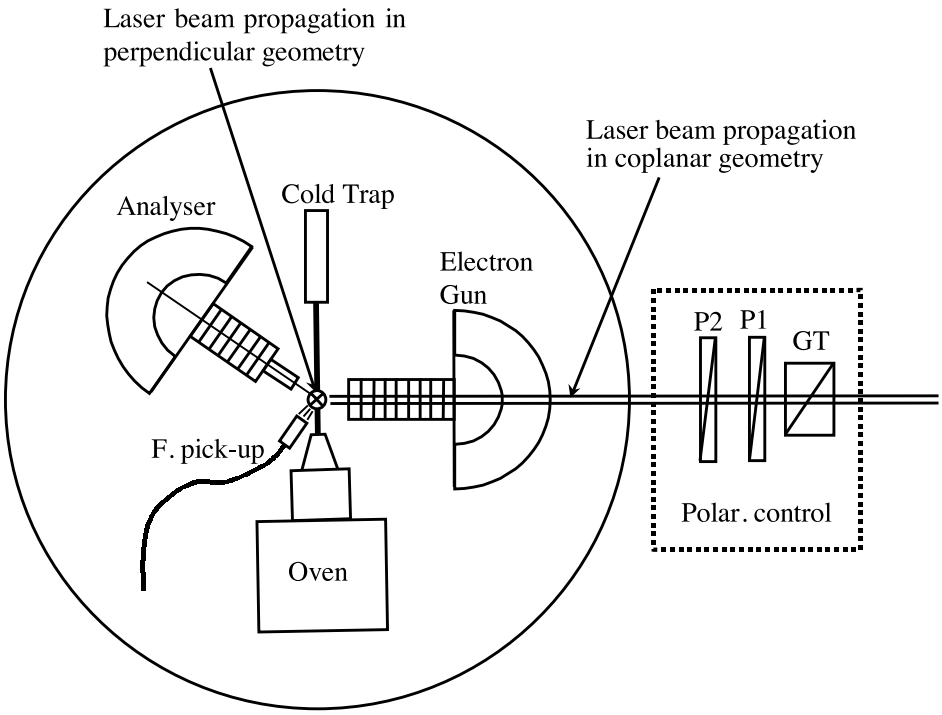

Figure 4. The schematic of the experimental set-up. The electron beam from the energy-selected electron gun and the laser beam intersect the atomic beam, produced by an atomic beam oven and dumped onto the cold trap. The rotatable scattered electron analyser detects the scattered electrons with the appropriate energy loss at different scattering angles. The fluorescence pick-up (F. pick-up) collects the fluorescence emitted by the laser-excited atoms to monitor the laser frequency tuning. The polarization control unit contains a Glan–Taylor polarizer (GT) and two quarter-wave plates (P1 and P2) which set the laser light polarization. In co-planar laser excitation geometry the laser beam is propagated through the electron gun along the incident electron beam.

perpendicular to the laser beam in both the perpendicular and co-planar laser excitation geometries (figure 4).

Optical excitation of the sodium atoms was accomplished by using 589 nm radiation from two CW single-mode dye lasers (Spectra Physics 380D), pumped by a 20 W Ar-ion laser (Coherent Innova 420). Two laser modes were tuned to excite from the $F = 2$ and $F = 1$ substates of the ground $3S_{1/2}$ state. Such an excitation scheme allows the highest excited state population to be obtained, thus increasing the scattering signal and providing a more uniform distribution of the excited atoms in the interaction region (Shurgalin *et al* 1998). At the same time, a higher laser intensity can be used to reduce the sensitivity of the optical pumping parameters to small laser frequency detuning.

The two laser beams are combined using a 50/50 beamsplitter. When measuring the P_1^S, P_2^S and P_3^S pseudo-Stokes parameters, the perpendicular laser excitation geometry is required and the laser beam is propagated through a viewport on the top of the vacuum chamber. When measuring the P_4^S parameter, the laser beam is propagated through a viewport on the side of the vacuum chamber and through the electron gun. A small hole

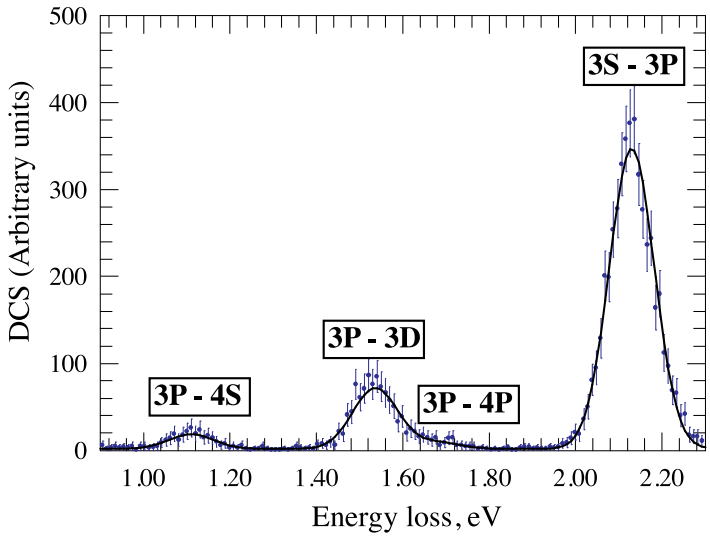

Figure 5. Energy loss spectrum showing peaks corresponding to 3P–4S, 3P–3D, 3P–4P and 3S–3P transitions in atomic sodium.

was made for this purpose at the back of the larger hemisphere of the electron gun energy selector. Some aperturing of the laser beam occurred, but it was possible to create the same optical pumping conditions in both geometries. This was carefully checked by measuring the value of the optical pumping parameter in both laser excitation geometries by the fluorescence polarization technique (Farrell *et al* 1991) and finding it to be the same within experimental error. The laser light polarizations required for measuring pseudo-Stokes parameters were obtained using three optical elements as shown in figure 4. A Glan–Taylor prism is used to clean up the original laser polarization, the first quarter-wave plate is used to create circular polarizations for measuring the P_3^S parameter and the second quarter-wave plate in combination with the first plate is used to create the required linear polarizations.

Much care and attention was given to the alignment of the electron spectrometer. Zero scattering angle and the accuracy of the geometrical alignment were checked by recording the elastic scattering signal from an Ar atomic beam as a function of scattering angle for both positive and negative scattering angles. The Ar beam was aligned perpendicular to the scattering plane to ensure symmetry of the Ar atomic density with respect to the scattering angle. Also, the symmetry with respect to positive and negative scattering angles for measured pseudo-Stokes parameters for the sodium atomic beam indicated good alignment. To calibrate the incident electron energy, the Ar atomic beam was replaced with a He atomic beam and the energy was calibrated using known resonances in the range 20–24 eV for electron-impact excitation of metastable $2\,^3$S and $2\,^1$S helium atoms (Buckman *et al* 1983).

To monitor the frequency tuning of the lasers during the experiment, fluorescence emitted by excited atoms is collected and delivered via an optical fibre to a photomultiplier tube located outside the vacuum chamber. Laser tuning was adjusted to maximize the fluorescence signal.

When measuring pseudo-Stokes parameters, as in the case of the standard Stokes parameters, the detector efficiency, target atom density and incident electron beam current do not influence the measured pseudo-Stokes parameters. Only the relative signal differences for different laser polarizations are taken into account. However, it is very important to ensure the stability of these experimental conditions during each pseudo-Stokes parameter measurement. In a real experimental situation, some variations are inevitable and therefore in each measurement a test for stability is required. This is accomplished by analysing the magnitude of the signal corresponding to the inelastic 3S–3P scattering from the ground state. Since this signal does not depend on laser polarization used in obtaining each pseudo-Stokes parameter, it therefore must remain constant if the target atom density, incident electron beam current and detector efficiency remain stable. Because the 3S–3P transition is depopulated by laser excitation, this reference signal also reflects the stability of optical pumping including the stability of mutual alignment of the laser and electron beams. Comparing the magnitudes of the reference signals for different laser polarizations in each pseudo-Stokes parameter measurement provides a continuous test for stability. If the reference signals differed by more than two standard deviations then the measurement was rejected and the system checked. In most cases laser detuning, which was also indicated by a change in fluorescence intensity, and electron gun instability were responsible for variations in the reference signal.

4. Results and discussion

Figure 6 shows the four measured pseudo-Stokes parameters as functions of scattering angle. These raw data already give some information on the collision process. At small scattering angles up to about 12°–14° the P_1^S, P_2^S and P_4^S parameters are small, while the P_3^S parameter, which is related to the angular momentum transfer $L_\perp$, is comparatively large. This indicates that transitions involving the $m = +1$ substate of the P-state are significantly favoured at small positive scattering angles, similar to the excitation of the 3P-state of sodium from the ground 3S-state (McClelland *et al* 1987, Sang *et al* 1994 and references therein). Transitions populating the $m = 0$ substate are also significant in this range since the P_4^S parameter is almost zero at 6° and 10° scattering angles, thus indicating that a large volume of the charge cloud lies out of the scattering plane.

A clearer picture emerges when the density matrix elements of the P-state are calculated, which give the sums of MSEPs, given by equation (12). The following values for the optical pumping parameters, obtained from the quantum electrodynamics model of the optical excitation of the 3P-state of sodium, were used in the calculation: $K_L = 0.36$, $K_c = 0.99$ and $K_c'' = 0.95$. The K_L parameter was also verified experimentally as mentioned in the previous section.

Figure 7 presents the experimentally obtained MSEP sums as functions of scattering angle and the result of a CCC theoretical calculation (Bray 1998). Full details of the CCC have been presented in Bray *et al* (1994). Good agreement between the experimental results and the CCC theory is evident at all scattering angles. At 0° scattering angle, the values of the excitation probabilities $(\sigma_{-21} + \sigma_{01} + \sigma_{21})$, $(\sigma_{-10} + \sigma_{10})$ and $(\sigma_{-2-1} + \sigma_{0-1} + \sigma_{2-1})$ are within the range 0.3–0.36, suggesting that all magnetic substates of the 3P state contribute almost equally to the excitation of the 3D state. In the range of scattering angles from 0° to 10°, the probability of transitions between magnetic substates of negative reflection symmetry, that is the $m = 0$ substate of the 3P-state and the $m = \pm 1$ substates of the 3D-state, given by $\rho_{00}^{3P(e)}$ does not vary significantly, remaining within the range 0.3–0.34. This value is comparable with the probability of transitions between magnetic substates of

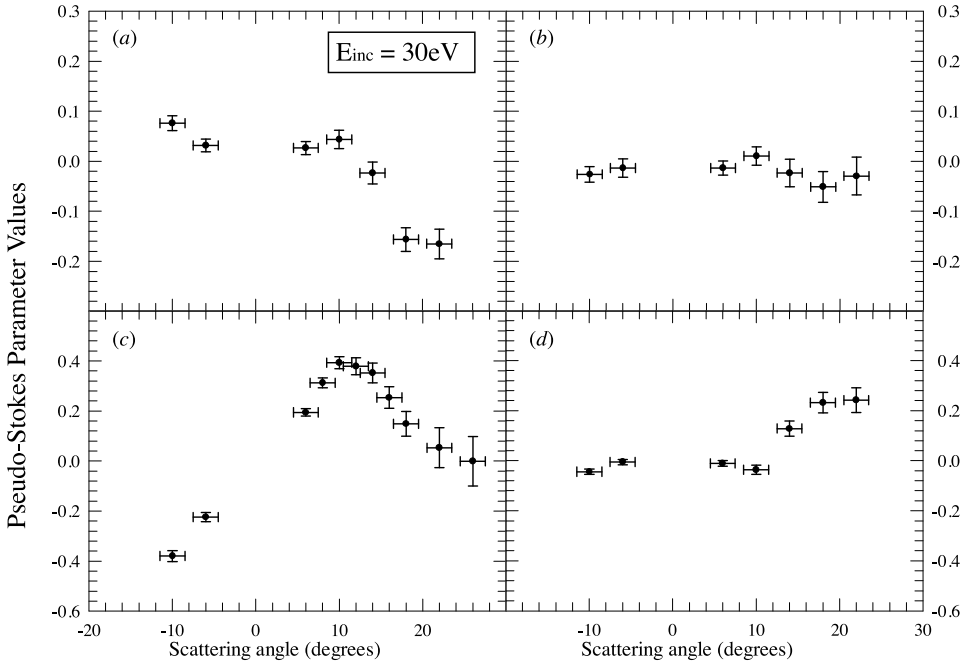

Figure 6. (*a*) P_1^S, (*b*) P_2^S, (*c*) P_3^S and (*d*) P_4^S parameters as functions of scattering angle measured at 30 eV incident electron energy for the 3P–3D transition.

positive reflection symmetry. While there are three scattering amplitudes contributing to transitions between magnetic substates of positive reflection symmetry, there are only two scattering amplitudes contributing to transitions between magnetic substates of negative reflection symmetry and therefore the latter transitions are quite favoured in this range of scattering angles. However, as the scattering angle increases, transitions between magnetic substates of negative reflection symmetry become much less significant as indicated by a decrease in the value of $\rho_{00}^{3P(e)}$ to less than 0.1 at 22°. At the same time, an interesting trend is observed for transitions between magnetic substates of positive reflection symmetry. At small and positive scattering angles the $m = 1$ substate of the 3P-state contributes to the 3D-state excitation more than the $m = -1$ substate. The maximum difference is reached at a scattering angle of about 12°. Beyond this angle the difference becomes less significant and at scattering angles from 22° to 24°, both the $m = -1$ and $m = 1$ substates contribute to the excitation process almost equally. Considering the 3P–3D scattering process in terms of excitation of the 3P-state from the isotropic 3D-state this trend is also clearly indicated by the behaviour of the standard $L_\perp$ parameter.

When excitation of the 3P-state from the 'isotropic' 3D-state is considered, the standard ACPs $L_\perp$, ρ_{00}^{nat}, P_ℓ and γ can be used (Andersen *et al* 1988). These parameters are related to the density matrix elements of the P-state in the following way:

$$L_\perp = \rho_{11}^{3P(e)} - \rho_{-1-1}^{3P(e)} \qquad \rho_{00}^{\mathrm{nat}} = \rho_{00}^{3P(e)}$$
$$P_\ell = \left|\rho_{1-1}^{3P(e)}\right| \qquad \text{and} \qquad \gamma = \frac{1}{2}\arctan\left(\frac{\mathrm{Im}\left(\rho_{1-1}^{3P(e)}\right)}{\mathrm{Re}\left(\rho_{1-1}^{3P(e)}\right)}\right). \tag{29}$$

Figure 8 presents both the experimental values and the CCC calculation of the $L_\perp$ (*a*), P_ℓ

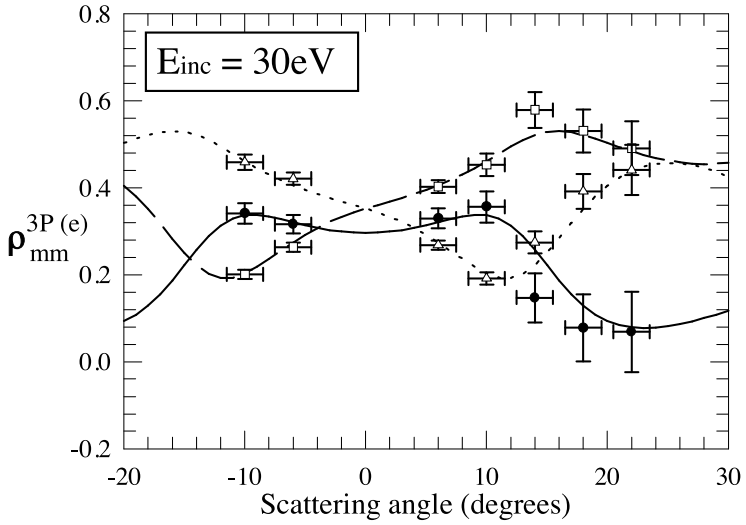

Figure 7. Density matrix elements $\rho_{11}^{3P(e)}$ (squares and broken curve), $\rho_{00}^{3P(e)} = \rho_{00}^{\rm nat}$ (circles and full curve) and $\rho_{-1-1}^{3P(e)}$ (triangles and dotted curves) giving magnetic substate excitation probabilities for the 3P–3D excitation as functions of scattering angle at 30 eV incident electron energy. Curves represent the convergent close-coupling theory calculations of Bray (1988).

(b) and γ (c) parameters as functions of scattering angle and the $\rho_{00}^{\rm nat}$ parameter is shown in figure 7. The experimental $L_\perp$ and P_ℓ are calculated from

$$L_\perp = \frac{1 - K_c'' \rho_{00}^{3P(e)}}{K_c} P_3^S \qquad \text{and} \qquad P_\ell = \sqrt{\left(\rho_{00}^{3P(e)} - \frac{1}{K_L}\right)^2 \left(P_1^2 + P_2^2\right)}. \tag{30}$$

For all these parameters, the CCC theory provides good agreement with the experiment, being in excellent agreement at all scattering angles for the $L_\perp$ parameter. The $L_\perp$ parameter is positive and increases with scattering angle in the range from 0° to $+15^\circ$, reaching a maximum of ~ 0.3 and then decreases to a very small value at about 22°. The P_ℓ parameter is very small in the range of scattering angles from 0° to $+15^\circ$, which is correlated with the relatively large values of $\rho_{00}^{\rm nat}$ (charge cloud 'height' parameter, Andersen *et al* (1988)) and then increases to ~ 0.5 at 22° scattering angle as $\rho_{00}^{\rm nat}$ decreases. The γ parameter is nearly zero at small scattering angles from 6° to 10° and then changes quite rapidly, being almost 90° at scattering angles of 18° and 22°.

It is interesting to analyse the internal coherence of the excitation process for transitions between magnetic substates of positive reflection symmetry (Andersen *et al* 1988). This degree of coherence is given by the P^+ parameter:

$$P^+ = \sqrt{P_\ell^2 + L_\perp^2}. \tag{31}$$

Figure 8(d) shows the P^+ parameter as a function of scattering angle. There is some degree of coherence observed, well below unity, at all scattering angles within the range from 0° to 22°. This is not surprising since three different scattering amplitudes contribute and these may not be in phase. There is a tendency for the coherence to increase slightly with scattering angle. This may indicate that out of three different scattering amplitudes one is possibly becoming more dominant. The CCC theory is again found to agree reasonably well

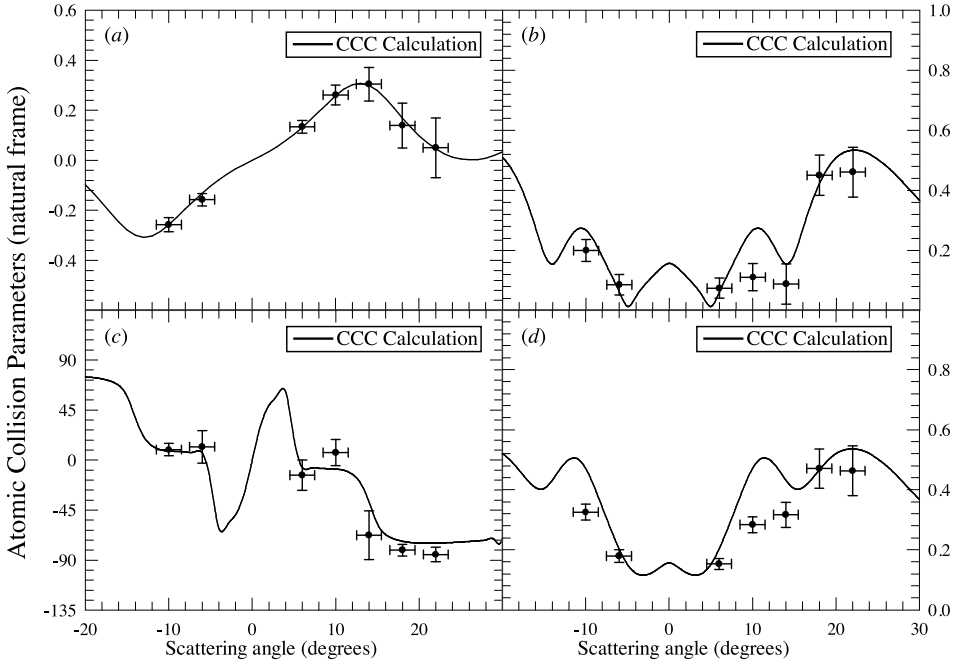

Figure 8. Angular momentum transfer $L_\perp$ (*a*), linear polarization of the P-state charge cloud P_ℓ (*b*), γ parameter (*c*) and P^+ parameter (*d*) as functions of scattering angle for the excitation of the 3P state from the isotropic 3D state at 28.4 eV incident electron energy. Curves show the convergent close-coupling theory calculations of Bray (1988).

with the experiment, however, there are smaller experimental values of the P^+ parameter observed at scattering angles of 10° and 14°.

The results obtained for the standard ACPs at 28.4 eV incident electron energy for the 3P state excitation from the isotropic 3D state of sodium appear to be similar to the results obtained at 5 eV incident electron energy for the same transition, presented in Andersen *et al* (1988). The only noticeable differences found are the following. At 5 eV incident electron energy the $L_\perp$ parameter reaches a maximum at a larger scattering angle $\sim 20^\circ$ and the $\rho_{00}^{\rm nat}$ and P_ℓ parameters vary with scattering angle more slowly in the range from 10° to 22°.

5. Conclusion

This work has presented a description of electron-impact-induced transitions between atomic states of different angular momenta for atoms which allow for conservation of the total electron spin, based on the density matrix formalism. Measurement schemes which allow the determination of some ACPs for excitation of the D-state from the P-state have been considered. It has been shown that measuring pseudo-Stokes parameters for the scattering signal from the laser-prepared P-state is equivalent to studying the electron-impact excitation of the P-state from the isotropic D-state. At the same time, this method allows the determination of certain sums of MSEPs for the electron-impact-induced P- to D-state transition.

The experiment of electron scattering from the optically prepared 3P-state of sodium has been described. The P_1^S, P_2^S, P_3^S and P_4^S pseudo-Stokes parameters have been measured for the 3P–3D transition. These allow the determination of probabilities of excitation of the 3D-state from a particular magnetic substate of the 3P-state, which are given by certain sums of MSEPs. These probabilities are believed to provide more comprehensive tests of theory and give more information about the collision dynamics involved in the electron-impact excitation of the D-state from the P-state, than DCS measurements alone. The experimental data are compared with the CCC theory calculations. Good agreement between the theory and the experiment is found, in support of the applicability of the CCC theory for electron-impact-induced transitions between excited atomic states of higher angular momenta and at higher incident electron energies than have previously been considered.

Acknowledgments

The authors would like to thank Dr I Bray for providing the CCC calculation results. Financial support for this work was provided by the Australian Research Council. One of us (MS) was supported by a Griffith University Postgraduate Award.

Appendix

In this appendix the derivation of the general formula describing electron-impact-induced transitions allowing conservation of the total electron spin is outlined. The derivation follows closely that of Blum (1981). An ensemble of target atoms in an initial state immediately prior to the collision is described by the atomic density operator ρ^A:

$$\rho^A = \frac{1}{2S_0+1}\sum_{M_{S_0}} |\alpha_0\, L_0\, M_{L_0}\, S_0\, M_{S_0}\rangle\langle\alpha_0\, L_0\, M_{L_0}\, S_0\, M_{S_0}| \tag{A1}$$

where S_0 and M_{S_0} are the atomic electron spin quantum numbers, L_0 and M_{L_0} are orbital angular momentum quantum numbers and α_0 denotes all other quantum numbers which are needed to fully specify the initial atomic state. All atoms have the same S_0, L_0 and α_0. Since no spins are observed, the initial atomic density operator is averaged over M_{S_0}. The initial state of the incident electrons, characterized by their linear momentum $\boldsymbol{P}_0$ and spin quantum number m_0, is described by the incident electron density operator ρ^e:

$$\rho^e = \tfrac{1}{2}\sum_{m_0} |\boldsymbol{P}_0\, m_0\rangle\langle\boldsymbol{P}_0\, m_0|. \tag{A2}$$

All electrons are assumed to have a well defined linear momentum $\boldsymbol{P}_0$. An average over the incident electron spin is taken because the incident electrons are not spin-polarized. Prior to the collision the target atoms and the incident electrons are two separate systems which are not correlated. The initial state of the combined system of the target atoms and the incident electrons can therefore be described by the density operator that is the direct product of the density operators for each separate system:

$$\rho^{(1)} = \rho^A X \rho^e = \frac{1}{2(2S_0+1)}\sum_{M_{S_0}\, m_0} |\alpha_0\, L_0\, M_{L_0}\, S_0\, M_{S_0}\, \boldsymbol{P}_0\, m_0\rangle\langle\alpha_0\, L_0\, M_{L_0}\, S_0\, M_{S_0}\, \boldsymbol{P}_0\, m_0|. \tag{A3}$$

Suppressing the dependence on the fixed variables $\alpha_0, L_0, S_0, \boldsymbol{P}_0$, the density matrix elements of $\rho^{(1)}$ are given by

$$\langle M'_{L_0}\, M'_{S_0}\, m_0|\rho^{(1)}|M_{L_0}\, M_{S_0}\, m_0\rangle = \frac{1}{2(2S_0+1)}\delta_{M'_{S_0}\, M_{S_0}}\langle M'_{L_0}|\rho^{A}|M_{L_0}\rangle. \tag{A4}$$

Immediately after the collision, the system of target atoms and scattered electrons are in a scattered state. This scattered state is described by the density operator $\rho^{(2)}$, which is related to the initial density operator by the transition operator $\boldsymbol{T}$:

$$\rho^{(2)} = \boldsymbol{T}\rho^{(1)}\boldsymbol{T}^{+}. \tag{A5}$$

Let the quantum numbers $\alpha_1, L_1, M_{L_1}, S_1, M_{S_1}$ and $\boldsymbol{P}_1, m_1$ characterize the final state $\rho^{(2)}$. The scattered electrons are detected only with a particular linear momentum $\boldsymbol{P}_1$, corresponding to an energy loss for the excitation of a particular atomic state, which is characterized by well defined quantum numbers α_1, L_1 and S_1. The resolution of an electron spectrometer can usually be made good enough to resolve individual transitions into the states of different α_1, L_1 and S_1 (e.g. singlet and triplet states). Due to such selection α_1, L_1 and S_1 are the same for all atoms excited by the collisions with the detected electrons. Hence the dependence of $\rho^{(2)}$ on these terms can be suppressed. The density matrix elements of $\rho^{(2)}$ are then given by

$$\langle M'_{L_1} M'_{S_1} m'_1|\rho^{(2)}|M_{L_1} M_{S_1} m_1\rangle = \langle M'_{L_1} M'_{S_1} m'_1|\boldsymbol{T}\rho^{(1)}\boldsymbol{T}^{+}|M_{L_1} M_{S_1} m_1\rangle. \tag{A6}$$

Using the 'completeness' relation (Blum 1981):

$$\sum_{M_{L_0} M_{S_0} m_0} |M_{L_0} M_{S_0} m_0\rangle\langle M_{L_0} M_{S_0} m_0| = 1 \tag{A7}$$

the following equation is obtained:

$$\begin{aligned}\langle M'_{L_1} M'_{S_1} m'_1|\rho^{(2)}|M_{L_1} M_{S_1} m_1\rangle = &\sum_{M'_{L_0} M_{L_0} M'_{S_0} M_{S_0} m'_0 m_0} \langle M'_{L_1} M'_{S_1} m'_1|\boldsymbol{T}|M'_{L_0} M'_{S_0} m'_0\rangle \\ &\times\langle M'_{L_0} M'_{S_0} m'_0|\rho^{(1)}|M_{L_0} M_{S_0} m_0\rangle\langle M_{L_0} M_{S_0} m_0|\boldsymbol{T}^{+}|M_{L_1} M_{S_1} m_1\rangle.\end{aligned} \tag{A8}$$

Substituting expression (A4) for the $\rho^{(1)}$ density matrix elements into equation (A8) and taking an average over the unobserved spins, the following equation is obtained:

$$\begin{aligned}\langle M'_{L_1}|\rho^{(2)}|M_{L_1}\rangle &= \sum_{M_{S_1} m_1} \langle M'_{L_1} M_{S_1} m_1|\rho^{(2)}|M_{L_1} M_{S_1} m_1\rangle \\ &= \sum_{M'_{L_0} M_{L_0}} \langle M'_{L_0}|\rho^{(1)}|M_{L_0}\rangle \frac{1}{2(2S_0+1)} \\ &\quad\times \sum_{M_{S_1} m_1 M_{S_0} m_0} \langle M'_{L_1} M_{S_1} m_1|\boldsymbol{T}|M'_{L_0} M_{S_0} m_0\rangle\langle M_{L_0} M_{S_0} m_0|\boldsymbol{T}^{+}|M_{L_1} M_{S_1} m_1\rangle.\end{aligned} \tag{A9}$$

The resulting $\rho^{(2)}$ is the reduced density matrix that describes only the orbital states of an ensemble of electron-impact excited atoms. The matrix elements of the transition operator in the above equation can be recognized as the scattering amplitudes. These scattering amplitudes still have a dependence on spin components. Using the conservation of total spin and angular momenta, the expression for $\rho^{A(2)}$ matrix elements can be obtained, which involves spin-averaged scattering amplitudes depending only on the orbital quantum numbers (Blum 1981). States with different atomic and projectile electron spins are related

to the states of total spin S, m_S through the Clebsch–Gordan coefficients. Using these coefficients the transition matrix elements can be re-cast into the following form:

$$\langle M'_{L_1} M'_{S_1} m'_1 | \boldsymbol{T} | M'_{L_0} M_{S_0} m_0 \rangle = \sum_{S' M'_S} \langle \tfrac{1}{2}, \tfrac{1}{2}, M_{S_0}, m_0 | (\tfrac{1}{2}, \tfrac{1}{2}) S', M'_S \rangle \langle \tfrac{1}{2}, \tfrac{1}{2}, M_{S_1}, m_1 | (\tfrac{1}{2}, \tfrac{1}{2}) S', M'_S \rangle$$
$$\times \langle S' M'_S M'_{L_1} | \boldsymbol{T} | S' M'_S M'_{L_0} \rangle \qquad \text{(A10}a\text{)}$$

and

$$\langle M_{L_0} M_{S_0} m_0 | \boldsymbol{T}^+ | M_{L_1} M_{S_1} m_1 \rangle = \sum_{S M_S} \langle \tfrac{1}{2}, \tfrac{1}{2}, M_{S_0}, m_0 | (\tfrac{1}{2}, \tfrac{1}{2}) S, M_S \rangle$$
$$\times \langle \tfrac{1}{2}, \tfrac{1}{2}, M_{S_1}, m_1 | (\tfrac{1}{2}, \tfrac{1}{2}) S, M_S \rangle \langle S M_S M_{L_0} | \boldsymbol{T}^+ | S M_S M_{L_1} \rangle \qquad \text{(A10}b\text{)}$$

where expressions of the form $\langle \frac{1}{2}, \frac{1}{2}, M_{S_0}, m_0 | (\frac{1}{2}, \frac{1}{2}) S', M'_S \rangle$ denote the Clebsch–Gordan coefficients. Substituting (A10) into (A9) and using the unitary properties of the Clebsch–Gordan coefficients yields

$$\langle M'_{L_1} | \rho^{A(2)} | M_{L_1} \rangle = \sum_{M_{L_0} M'_{L_0}} \langle M'_{L_0} | \rho^{A(1)} | M_{L_0} \rangle \frac{1}{2(2S_0 + 1)} \sum_S (2S + 1) \langle S M'_{L_1} | \boldsymbol{T} | S M'_{L_0} \rangle$$
$$\times \langle S M_{L_0} | \boldsymbol{T}^+ | S M_{L_1} \rangle \qquad \text{(A11)}$$

which contains spin-averaged transition operator matrix elements for each total spin channel. These transition matrix elements can be denoted as $T_{S,Mm}$ and $T^+_{S,nN}$, where M'_{L_1} and M'_{L_0} correspond to M and m subscripts, M_{L_1} and M_{L_0} correspond to N and n subscripts, S subscript denotes the total spin channel and $T^+_{S,nN} = T^*_{S,Nn}$ from the definition of the Hermitian conjugate (Messiah 1962). The probability of excitation through a particular total spin channel can be introduced as $W_S = (2S + 1)/2(2S_0 + 1)$. Equation (A11) can then be written in a compact matrix form:

$$\rho^{A(2)}_{MN} = \sum_{mn} \rho^{A(1)}_{mn} \sum_S W_S T_{S,Mm} T^*_{S,Nn} \qquad \text{(A12)}$$

where $\rho^{A(1)}_{mn}$ and $\rho^{A(2)}_{MN}$ are the density matrix elements describing the ensembles of atoms immediately before the collision and immediately after the collision, respectively.

References

Andersen N and Bartschat K 1996 *Adv. At. Mol. Opt. Phys.* **36** 1
——1997 *J. Phys. B: At. Mol. Opt. Phys.* **30** 5071
Andersen N, Bartschat K, Broad J T and Hertel I V 1997a *Phys. Rep.* **279** 251
Andersen N, Broad J T, Campbell E E B, Gallagher J W and Hertel I V 1997b *Phys. Rep.* **278** 107
Andersen N, Gallagher J W and Hertel I V 1988 *Phys. Rep.* **165** 1
Blum K 1981 *Density Matrix Theory and Applications* (New York: Plenum)
Blum K and Kleinpoppen H 1979 *Phys. Rep.* **52** 203
Bray I 1998 Private communication
Bray I, Fursa D V and McCarthy I E 1994 *Phys. Rev.* A **49** 2667
Buckman S J, Hammond P, Read F H and King G C 1983 *J. Phys. B: At. Mol. Phys.* **16** 4039
Csanak G, Cartwright D C and Trajmar S 1992 *Phys. Rev.* A **45** 1625
Farrell P M, MacGillivray W R and Standage M C 1988 *Phys. Rev.* A **37** 4240
——1991 *Phys. Rev.* A **44** 1828
Hermann H W 1979 *Thesis* University Kaiserslautern, Kaiserslautern
Hermann H W and Hertel I V 1982a *Comment. At. Mol. Phys.* **12** 61
——1982b *Comment. At. Mol. Phys.* **12** 127
Hummer C R and Burns D J 1986 *Phys. Rev.* A **33** 2995
Kessler J 1985 *Polarized Electrons* (Berlin: Springer)

Li Y, Wang S, Zetner P W and Trajmar S 1994 *J. Phys. B: At. Mol. Opt. Phys.* **27** 4025
Li Y and Zetner P W 1995 *J. Phys. B: At. Mol. Opt. Phys.* **28** 5151
——1996 *J. Phys. B: At. Mol. Opt. Phys.* **29** 1803
Lin C C and Anderson L W 1992 *Adv. At. Mol. Opt. Phys.* **29** 1
Macek J and Hertel I V 1974 *J. Phys. B: At. Mol. Opt. Phys.* **7** 2173
MacGillivray W R and Standage M C 1991 *Comment. At. Mol. Phys.* **26** 179
McClelland J J, Kelley M H and Celotta R J 1987 *J. Phys. B: At. Mol. Phys.* **20** L385
Meng X-K, MacGillivray W R and Standage M C 1992 *Phys. Rev.* A **45** 1767
Messiah A 1962 *Quantum Mechanics* (New York: Wiley)
Sang R T, Farrell P M, Madison D H, MacGillivray W R and Standage M C 1994 *J. Phys. B: At. Mol. Opt. Phys.* **27** 1187
Shurgalin M, Farrell P M and MacGillivray W R 1998 in preparation
Stumpf B and Gallagher A 1985 *Phys. Rev.* A **32** 3344
Trajmar S and Nickel C R 1993 *Adv. At. Mol. Opt. Phys.* **30** 45
Verma S and Srivastava R 1996 *J. Phys. B: At. Mol. Opt. Phys.* **29** 3215
Zetner P W, Trajmar S, Wang S, Kanik I, Csanak G, Clark R E H, Abdallah J and Nickel J C 1997 *J. Phys. B: At. Mol. Opt. Phys.* **30** 5317